RSC Advances

PAPER

View Article Online
View Journal | View Issue

Cite this: *RSC Adv.*, 2020, **10**, 19247

Abiotic reduction of *p*-chloronitrobenzene by sulfate green rust: influence factors, products and mechanism†

Ying Han, Junkai Huang, Hongyuan Liu,* Yue Wu, Zhao Wu, Kemin Zhang and Qingjie Lu

Received 6th March 2020
Accepted 13th May 2020

DOI: 10.1039/d0ra02113j

rsc.li/rsc-advances

The reduction of *p*-chloronitrobenzene (*p*-CNB) by sulfate green rust (GR_{SO_4}) was systematically studied. The results revealed that GR_{SO_4} has a good removal effect on *p*-CNB. The removal efficiencies of *p*-CNB by GR_{SO_4} improved with the increase of the pH value. The removal efficiencies in the presence of ions were better than that of GR_{SO_4} alone, while natural organic matter (NOM) could adsorb *p*-CNB, which competed with GR_{SO_4}. The reductions of *p*-CNB by GR_{SO_4} under different conditions followed pseudo-first-order reaction kinetics except for the reactions in the presence of NOM. *p*-CNB was converted into *p*-chloroaniline (*p*-CAN), which produced *p*-nitrosochlorobenzene and *p*-chlorophenylhydroxylamine as the intermediate products. The results of the X-ray diffraction (XRD), scanning electron microscopy (SEM) and transmission electron microscopy (TEM) showed GR_{SO_4} was gradually transformed into goethite. Fe(II) in the GR_{SO_4} structure was the main electron donor involved in the reaction.

Introduction

As a widely used raw material, *p*-chloronitrobenzene (*p*-CNB) is an important intermediate in the production of fine chemicals, pesticides, drugs and rubber.[1,2] Due to its high toxicity and strong bioaccumulation, *p*-CNB may cause cancer and affect the normal functioning of the central nervous system. If not disposed properly, it will eventually reach the aquatic environment and soil sediments, which poses a great threat to human beings and wildlife.[3–6] Therefore, it has been listed as a priority pollutant by many countries and regions.[7]

In recent decades, a lot of research has been carried out on the treatment of chlorinated nitrobenzene wastewater. The methods mainly include physical adsorption,[8] biodegradation,[9] advanced oxidation[10,11] and catalytic reduction.[12] The methods mentioned above have excellent removal efficiencies. However, the physical adsorption has difficulty in recovery. Biodegradation organisms are susceptible to interference with the concentration of substances. Advanced oxidation methods have the risks of secondary pollution and high cost, chemical stability and deactivation of the catalyst. In addition, due to the presence of strong electron withdrawing group chlorine substituent and nitro substituent on the aromatic ring, the oxidation processes require more energy.

In contrast, the chlorine substituent and the nitro substituent are thermodynamically favorable for the reduction reaction and enhance the *p*-CNB removal performance.[13] The application of catalytic reduction with H_2 may cause the concern of the safety of H_2 and the high price of catalyst. While, the natural subsurface anaerobic and hypoxic environment not only provide a variety of potential reduction conditions for the abiotic transformation of pollutants, but also provide reduction agents. For example, iron, as the fourth most abundant element in the earth's crust, is highly reductive in its elemental state and is often used as a reductant.[14,15] Although iron is a good reductant, in its natural state most of it exists as an oxide of iron.[16] Some minerals containing structural Fe(II) have been shown to reduce chlorinated hydrocarbons,[17] nitroaromatic hydrocarbons,[18] and pesticides.[19] Green rust (GR) as a kind of iron oxide with layered bimetallic hydroxide (LDH) structure,[20] obeys the general formula $[Fe^{II}_{(1-x)}Fe^{III}_{x}(OH)_2]^{x+}[(x/n)A^{n-}\cdot mH_2O]^{x-}$ including A^{n-} is anion intercalated (A^{n-} = Cl^-, SO_4^{2-}, CO_3^{2-}), m is the number of inserted water molecules and x is the molar fraction of Fe(III) {[Fe(III)]/[Fe(total)]}.[21,22] GR not only has good adsorption performance, but also has strong reduction ability.[23] The excellent reduction strength of GR is attributed to the high Fe(II) content and the rapid electron transfer between Fe(II) and Fe(III) in the hydroxide tablets by polaron jumps.[24] Due to its reductive reactivity and ability to absorb contaminants, GR suspension is considered a promising reductant for soil and groundwater remediation by *in situ* injection of GR into pollutant sources and plume.[25] The reductive transformation of *o*-chloronitrobenzene (*o*-CNB) by green rust was investigated, including reducing capacity of GR,

College of Civil Engineering and Architecture, Zhejiang University of Technology, Hangzhou 310023, P. R. China. E-mail: lhyzyy@zjut.edu.cn

† Electronic supplementary information (ESI) available. See DOI: 10.1039/d0ra02113j

effect of pH value, products and pathway. There were no kinetic studies, and the characterization of green rust was inadequate.[26] The reduction of *p*-CNB with Fe(II) bound to GR was investigated, mainly on the degradation kinetics.[16] There is a lack of the systematic study of *p*-CNB with GR solely. This study attempts to investigate the main influence factors on the reduction process of *p*-CNB removal by GR, the degradation products and explore the reaction mechanism.

Experimental

Chemicals

$FeCl_3 \cdot 6H_2O$ was purchased from Shanghai Lingfeng Chemical Reagent Co., Ltd. $FeSO_4 \cdot 7H_2O$ was purchased from Sinopharm Chemical Reagent Co., Ltd. NaOH and HCl were purchased from Xiqiao Science and Technology Co., Ltd. *p*-CNB, NaCl, $MgCl_2$, $CaCl_2$, KCl, Na_2SO_4, $NaHCO_3$, Na_2CO_3 and fulvic acid (FA) were purchased from Shanghai Aladdin Biotechnology Co., Ltd. Nitrobenzene, *p*-chloroaniline (*p*-CAN) and aniline were purchased from Shanghai Maclean Biotechnology Co., Ltd. All chemicals were used without further purification.

Mineral synthesis

The sulfate green rust (GR_{SO_4}) in this study was synthesized according to the previous method[27,28] of the co-precipitation of $FeCl_3 \cdot 6H_2O$ and $FeSO_4 \cdot 7H_2O$ in a glove box. 0.132 mol L^{-1} $FeSO_4 \cdot 7H_2O$ and 0.066 mol L^{-1} $FeCl_3 \cdot 6H_2O$ were added to 120 mL deoxygenated deionized water, stirring was continued until complete dissolution, 1 mol L^{-1} NaOH was dropwise titrated to the solution until the pH value reached 8.0. Then, solid and liquid separation was realized through suction filtration, and the filtered slurry was placed in a freeze-dried bottle, which was then freeze-dried. The dried powders were transferred to the glove box for grinding, and stored after 100 mesh screening. The obtained solid powders were confirmed to be GR_{SO_4} by X-ray diffraction (XRD) (Fig. 4a).

Reduction experiment

Reduction experiments were carried out in a glove box to test the ability of GR_{SO_4} to reduce *p*-CNB in an anaerobic environment. First, 0.1 g L^{-1} of GR_{SO_4}, 150 mL of deoxygenated deionized water, and 500 μg L^{-1} of *p*-CNB were sequentially added to a 150 mL conical flask. The conical flask was shaked on a horizontal shaker at 120 rpm for 40 min. 1 mL sample was got from the flask and filtrated through a 0.22 μm membrane to terminate the reaction at each time point. Then, the water sample was got for analysis. The solid powders were freeze-dried under N_2 protection and stored in a glove box for subsequent detection and characterization. The pH values of the deoxidized deionized water were adjusted first when the effects of initial pH value were investigated. For the experiments under different ions and NOM, ions or FA were added to water before *p*-CNB.

The reduction procedure of *p*-CNB by Fe(II) was as follows. Fe^{2+} stock solution was added to the 150 mL conical flask first, then the deoxidized deionized water and *p*-CNB were added into the flask. The following steps were the same as the reduction of *p*-CNB by GR_{SO_4}.

Analysis and characterization

p-CNB, *p*-CAN, nitrobenzene and aniline were analyzed by high performance liquid chromatography (HPLC, Agilent 1200). For *p*-CNB, the v/v ratios of water and methanol were 35 to 65, and the ultraviolet wavelength was 295 nm. For *p*-CAN, the v/v ratios of water and methanol were 35 to 65, and the ultraviolet wavelength was 240 nm. For nitrobenzene, the v/v/v ratios of methanol, water and acetic acid were 70, 29 and 1, and the ultraviolet wavelength was 262 nm. For aniline, the v/v ratios of water and methanol were 35 to 65, and the ultraviolet wavelength was 231 nm. The *p*-chlorophenylhydroxylamine and *p*-nitrosochlorobenzene were analyzed by gas chromatography mass spectrometry (GC-MS, Agilent 7980), the details were described in Text S1.† The concentrations of Fe(II) in the solution were determined by the 1,10-phenanthroline method.[29–31]

The solid powders before and after the reaction were characterized with X-ray diffraction (XRD, PANalytical B.V., X'Pert Pro) using Cu Kα radiation ($\lambda = 0.1541$ nm) at 40 kV and 40 mA, X-ray photoelectron spectroscopy (XPS, Shimadzu, KRATOS AXIS ULTRA DLD), scanning electron microscopy (SEM, ZEISS, GeminiSEM 300), and transmission electron microscopy (TEM, FEI, Tecnai G2 F30).

Kinetics

The kinetics of the *p*-CNB were described by a pseudo-first-order reaction (eqn (1)). C_0 is the initial concentration, C_t is the concentration at time t, t is the reaction time, and k_{obs} is the pseudo-first-order reaction rate constant.

$$\ln \frac{C_0}{C_t} = k_{obs} t \quad (1)$$

Results and discussion

Effect of initial pH value

The initial pH value is an essential factor which affects the reduction of *p*-CNB. The green rusts would be in varied states under different pH values and their abilities of reducing *p*-CNB are different. In this experiment, the pH values were set to 5.0, 6.5, 8.0 and 10.0, respectively, to investigate the effect of initial pH value on *p*-CNB reduction (Fig. 1). Interestingly, the final removals were higher with the increase of pH values. The pseudo-first-order reaction rates followed the same rule. The rates became higher with the increase of pH values (Table 1). This was significantly different from our common phenomena that lower pH values leaded to better reduction of pollutants with zero-valent iron (ZVI) and iron minerals.[32] However, the similar phenomena happened when GR was used to reduce *o*-CNB under the alkaline condition.[26] According to the Hayashi, this is caused by the different reactions of GR_{SO_4} at different pH values.[33] Besides, the rise of pH value could reduce the REDOX potential of green rust, thereby improving its reduction ability.[34]

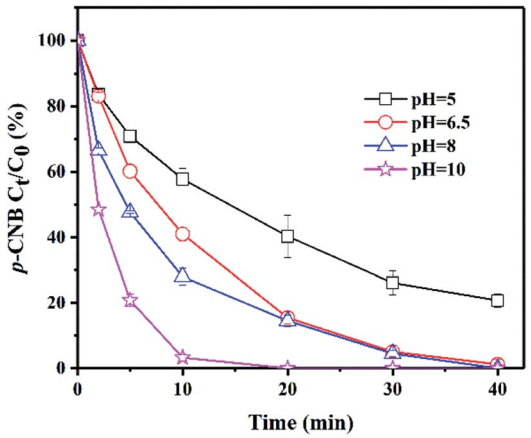

Fig. 1 Removal of *p*-CNB by GR_{SO_4} at different initial pH values. $[p\text{-CNB}]_0 = 500\ \mu g\ L^{-1}$, $[GR_{SO_4}]_0 = 0.1\ g\ L^{-1}$, $T = 20\ ^\circ C$. Error bars represent one standard deviation ($n = 3$).

Table 1 Reaction rates under different conditions ($[p\text{-CNB}]_0 = 500\ \mu g\ L^{-1}$, $[GR_{SO_4}]_0 = 0.1\ g\ L^{-1}$, $T = 20\ ^\circ C$)

Reaction conditions	k_{obs} ($\times 10^{-2}$)[a] (min^{-1})	R^2
pH = 5.0	4.28 ± 0.40	0.96
pH = 6.5	9.03 ± 0.46	0.99
pH = 8.0	10.49 ± 0.68	0.98
pH = 10.0	34.05 ± 3.10	0.99

[a] Uncertainties represent the standard deviation ($n = 3$).

Effect of ions and NOM

There are some inorganic or organic substances in the natural groundwater. Effect of several common ions (Na^+, K^+, Ca^{2+}, Mg^{2+}, Cl^-, SO_4^{2-}, HCO_3^-, CO_3^{2-}) and natural organic matter (NOM, fulvic acid) on the removal of *p*-CNB by GR_{SO_4} were investigated (Fig. 2). The final removals in the presence of cationic ions and anionic ions were similar to the system with GR_{SO_4} (Fig. 2a and b). All reaction rates were higher than GR_{SO_4} system (Table 2). All the cations showed positive effects on the reaction. The reaction rates were similar with small differences (Table 2). All cations were added to the reaction system in the form of chlorine salts. These electrolytes could facilitate electron transfer.[35] The higher rate in the presence of K^+ than that of Na^+ was caused by their conductivities.[35] This also worked for Ca^{2+} and Mg^{2+}. The systems containing Ca^{2+} and Mg^{2+} were better than that containing K^+ and Na^+. Because they have more moles of chlorine ions with the same mass concentration. The Cl^- could enhance the electron transfer.[35] The results of the system containing Cl^- also illustrated this (Table 2). The addition of SO_4^{2-} should also facilitate the electron transfer. However, the enhancement was just a little bit. This could be caused by the surface complexation of sulfate with green rust.[36] The improvement with HCO_3^- could be due to its enhancement on electron transfer and the effect of pH buffer.[37] In particular, the reaction rate of CO_3^{2-} system was significantly higher than

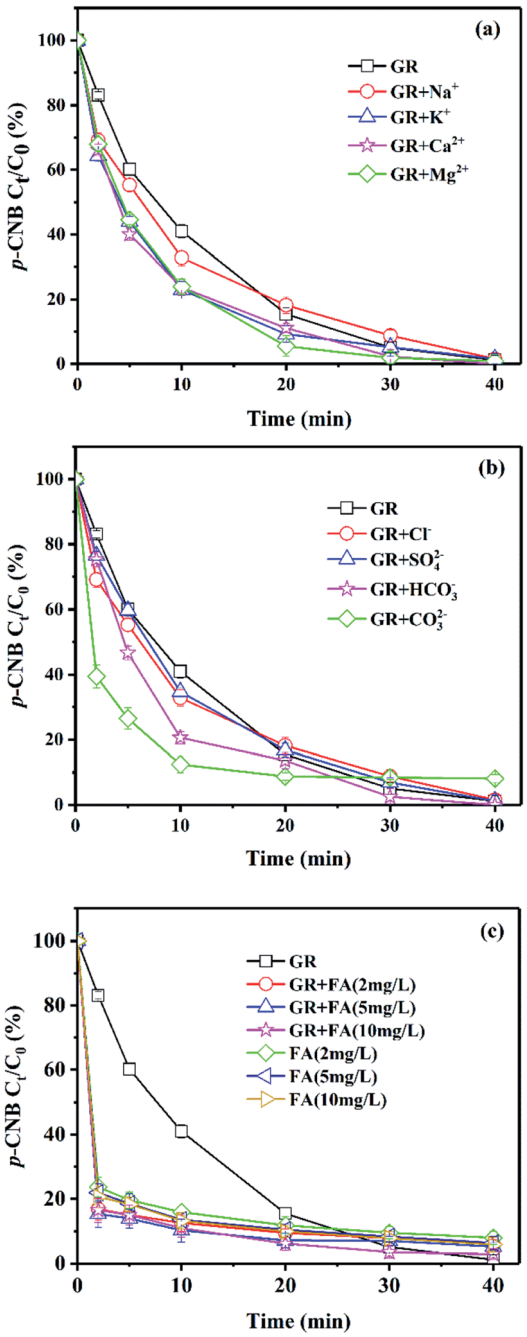

Fig. 2 Effect of (a) cationic ions, (b) anionic ions and (c) FA on the removal of *p*-CNB by GR_{SO_4}. $[p\text{-CNB}]_0 = 500\ \mu g\ L^{-1}$, $[GR_{SO_4}]_0 = 0.1\ g\ L^{-1}$, $T = 20\ ^\circ C$, pH = 6.5, $[Na^+]_0 = [K^+]_0 = [Ca^{2+}]_0 = [Mg^{2+}]_0 = [Cl^-]_0 = [SO_4^{2-}]_0 = [HCO_3^-]_0 = [CO_3^{2-}]_0 = 25\ mg\ L^{-1}$. Error bars represent one standard deviation ($n = 3$).

that of GR_{SO_4} system (Table 2). The increase of reaction rate in the system with CO_3^{2-} could be due to the substitution of SO_4^{2-} in GR_{SO_4} by CO_3^{2-}, resulting in the conversion of GR_{SO_4} to GR_{CO_3}.[38] GR_{CO_3} has lower reduction potential, and the pH value in the experiment increased due to the addition of CO_3^{2-}.[39] The reaction rate would also increase with increasing pH value as we discussed in the previous section (Fig. 1).

Table 2 Reaction rates under different ions ($[p\text{-CNB}]_0 = 500\ \mu g\ L^{-1}$, $[GR_{SO_4}]_0 = 0.1\ g\ L^{-1}$, $T = 20\ ^\circ C$, pH = 6.5, $[Na^+]_0 = [K^+]_0 = [Ca^{2+}]_0 = [Mg^{2+}]_0 = [Cl^-]_0 = [SO_4^{2-}]_0 = [HCO_3^-]_0 = [CO_3^{2-}]_0 = 25\ mg\ L^{-1}$)

Reaction conditions	k_{obs} ($\times 10^{-2}$)[a] (min^{-1})	R^2
GR only	9.03 ± 0.46	0.99
Na^+	11.75 ± 0.52	0.99
K^+	12.02 ± 0.48	0.98
Mg^{2+}	12.72 ± 0.56	0.99
Ca^{2+}	13.14 ± 0.72	0.99
Cl^-	11.75 ± 0.52	0.99
SO_4^{2-}	9.26 ± 0.68	0.99
HCO_3^-	12.74 ± 0.65	0.98
CO_3^{2-}	22.38 ± 2.80	0.89

[a] Uncertainties represent the standard deviation ($n = 3$).

Fulvic acid (FA) was used for the investigation of the effect of NOM. *p*-CNB was removed rapidly in a short time in the system of GR_{SO_4} with FA (Fig. 2c). The reactions did not follow the pseudo-first-order reaction kinetics. The removals of *p*-CNB with FA only were a little bit lower than that with FA and GR_{SO_4} (Fig. 2c). This indicated that the reaction mainly took place between *p*-CNB and FA, FA blocked the reduction reaction between GR_{SO_4} and *p*-CNB. FA had shown the adsorption capacity on TNT.[40] It is one component of humic acid (HA). HA had been used as the adsorbents for several organic contaminants.[41,42] The adsorption of *p*-CNB by FA could account for the rapid removal of *p*-CNB by FA in the absence and presence of GR_{SO_4}. HA could complex or oxidize on the GR surface and hinder the access of *p*-CNB.[37,43] The similar process may happen with FA. Therefore, the reduction of *p*-CNB by GR had been hindered. The small improvements for the *p*-CNB removals in the presence of GR_{SO_4} and FA could be due to their joint effects.

Products

Based on the structure of *p*-CNB, it is expected to undergo nitro reduction and dechlorination. Possible products include nitrobenzene, aniline, *p*-nitrosochlorobenzene, *p*-chlorophenylhydroxylamine, *p*-CAN and chloride ions. Nitrobenzene and aniline were not detected. Therefore, GR_{SO_4} could not dechlorinate *p*-CNB. *p*-CAN was the final product, which was similar as the former study on *o*-CNB.[26] The concentration of *p*-CAN gradually increased with the decrease of the concentration of *p*-CNB (Fig. 3). But the total amount of nitrogen were unbalanced in the intermediate time periods. The removal of *p*-CNB basically completed in the reaction period of 40 minute, but *p*-CAN did not generate as much, indicating that the reaction was still going on. All *p*-CNB was converted to *p*-CAN after 120 min. The nitrogen loss should be due to the existence of the intermediate products. *p*-chlorophenylhydroxylamine was found (Fig. S1†). No *p*-chloronitrosobenzene was detected. Its existence time should be extremely short, which could be

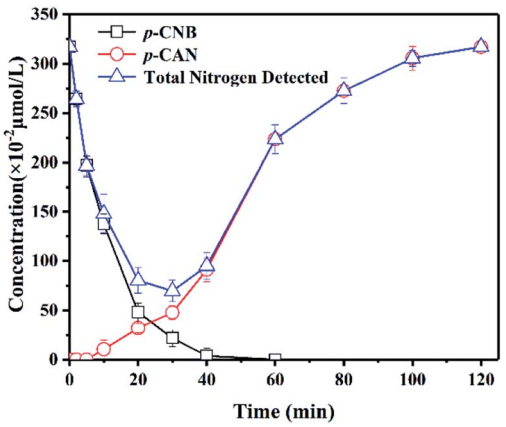

Fig. 3 Products of the removal of *p*-CNB by GR_{SO_4}. $[p\text{-CNB}]_0 = 3.17\ \mu mol\ L^{-1} = 500\ \mu g\ L^{-1}$, $[GR_{SO_4}]_0 = 0.1\ g\ L^{-1}$, $T = 20\ ^\circ C$, pH = 6.5. Error bars represent one standard deviation ($n = 3$).

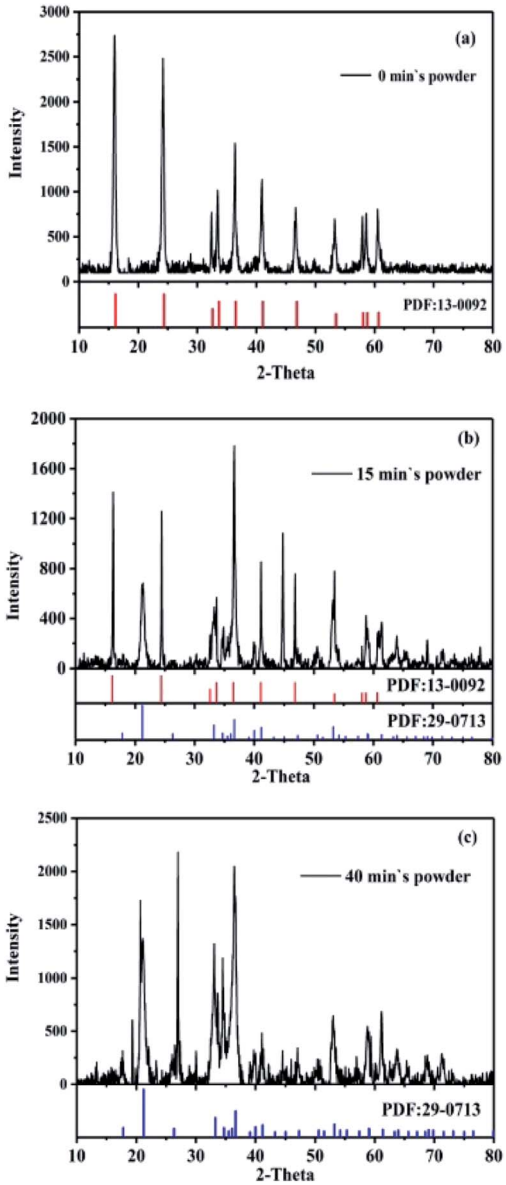

Fig. 4 XRD pattern of GR_{SO_4} powders at (a) 0 min, (b) 15 min and (c) 40 min.

quickly reduced to *p*-chlorophenylhydroxylamine.[16,44] This was similar to the reduction of nitrobenzene with Fe(II).[44]

Characterization of GR_{SO_4} powders

In order to observe the changes of phase compositions, surface morphologies and internal structures of GR_{SO_4} powders before and after the reaction, the GR_{SO_4} powders were analyzed by XRD, SEM and TEM. The XRD patterns were collected with a 2θ range from 10° to 80° at a step of 0.05°. The average crystallite sizes of the samples were calculated with the Scherrer equation based on the strongest *hkl* (002) diffraction peak of green rust. The results (Fig. 4) showed that the mineral powders converted from GR_{SO_4} (Fig. 4a, PDF#13-0092, JCPDS) to goethite (Fig. 4c, PDF#29-0713, JCPDS). There was still unreacted GR_{SO_4} in the presence of goethite after 15 min reaction (Fig. 4b). Goethite was also detected when *o*-CNB was reduced by GR, many other kinds of iron minerals were detected.[26] However, only goethite was detected in this study. Through SEM images we directly saw that GR_{SO_4} had a smooth layered structure, and the surface grew into strip crystals at 15 min, and finally became strip crystals at 40 min (Fig. S2†). In the low resolution TEM (Fig. 5), the similar phenomena occurred as the SEM (Fig. S2†), and the black part seen in Fig. 5a was due to the fact that the sample concentration was so high that the mineral particles were stacked and the GR particles were 90° away from the TEM probe. In the high resolution TEM after fourier transformation, the powders at 0 min were amorphous and the crystal structure was disordered (Fig. 5d). The powders at 40 min was polycrystalline (Fig. 5e). After the fourier transformation into concentric rings, the crystal structure was in a staggered and orderly state. After measuring the interplanar spacing in Fig. 5d, we found that it coincided with the 100 crystal plane of GR_{SO_4} (PDF#13-0092, JCPDS), and Fig. 5e coincided with the 130 crystal plane of goethite (PDF#29-0713, JCPDS). The results were consistent with those of XRD.

The surface chemical properties of the unreacted GR_{SO_4} powders, the GR_{SO_4} powders at 15 min and 40 min were analyzed by XPS. According to the spectra of the unreacted GR_{SO_4} powders, Fe and O were found on the surface of the samples, as well as a small amount of residual S (about 3%) (Table S1†). The iron to oxygen ratio determined from utilising the peak area and sensitivity factor was close to 0.4 (Table S1 and eqn (S1)†), which was consistent with the Mullet.[21]

In order to further understand the changes of iron composition in GR_{SO_4} before and after the reaction, spectral fitting is required. The fitting process of Fe (2p) domain spectra of iron (oxyhydro) oxides is usually complex, including multiple contributions and satellite characteristics.[45] In mixed valence compounds, the complexity is enhanced by overlapping multiple peaks of Fe(II) and Fe(III) species.[46] It was shown that the multiple peaks calculated by Gupta and Sen could well fit the Fe ($2p_{3/2}$) peaks in Fe(II) and Fe(III) compounds.[47] Therefore, they were used to study the changes of GR_{SO_4} before and after reaction (Fig. 6, Tables S2 and S3†). When GR_{SO_4} was not reacted, the photoelectron peaks of Fe (2p) and O (1s) were respectively at 710.9 ev and 531.4 ev. The Fe(II)/Fe(III) ratio of 2.0, and it was consistent

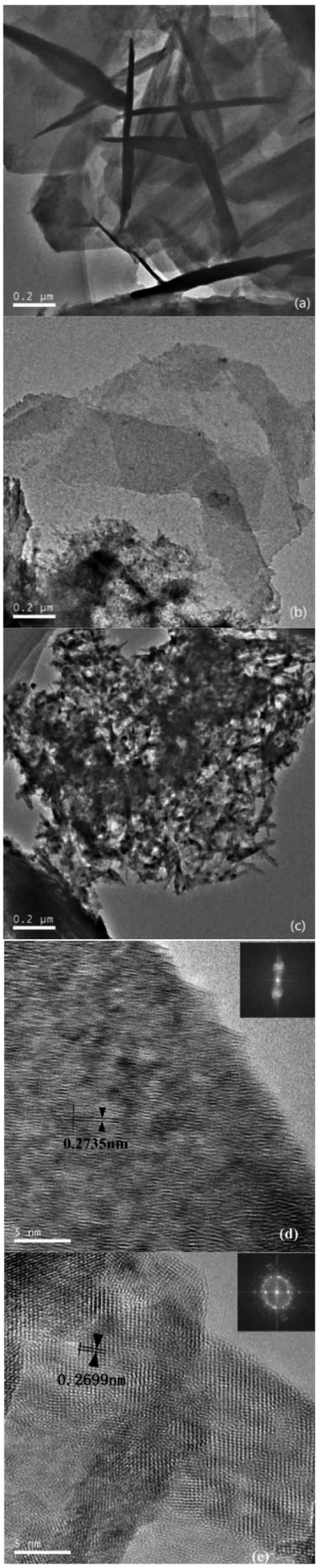

Fig. 5 TEM of powders at (a) 0 min, (b) 15 min and (c) 40 min and high-resolution TEM of powders at (d) 0 min and (e) 40 min.

with the results reported by Perez *et al.*[48] The shape and position of Fe ($2p_{3/2}$) photoelectron peaks were also similar to the previously reported XPS spectra of GR_{SO_4}.[48] In addition, the relative

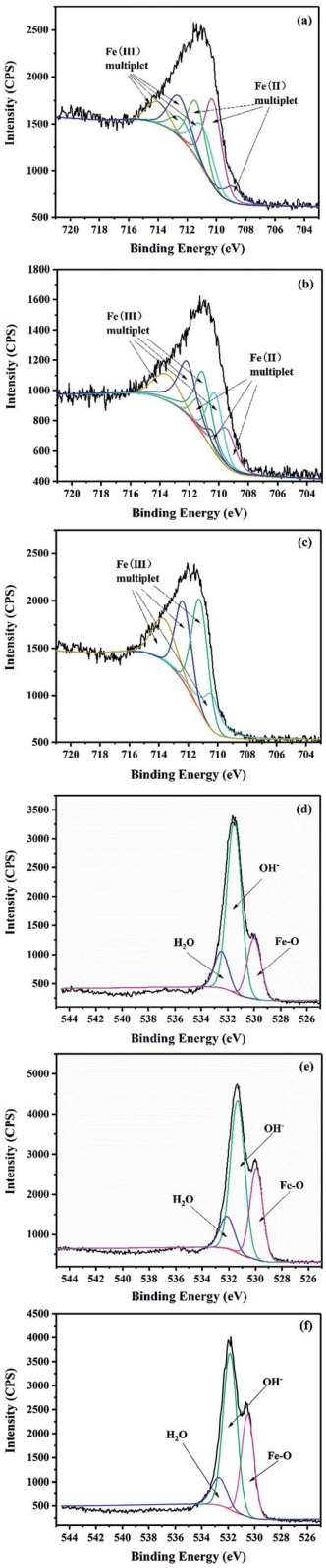

Fig. 6 Fe $2p_{3/2}$ spectra of powders (a) unreacted, (b) 15 min, (c) 40 min and O 1s spectra of powders (d) unreacted, (e) 15 min, (f) 40 min.

values of Fe–O, O–H and adsorbed water of the O (1s) peak were 529.9, 531.3 and 532.1 eV, respectively (Fig. 6d and Table S3†), which were consistent with the values obtained by Mullet *et al.*[21]

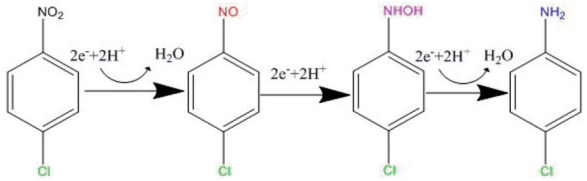

Fig. 7 Reaction process of the reduction of *p*-CNB by GR_{SO_4}.

After the reaction, the photoelectron peaks of Fe (2p) and O (1s) all changed, in particular, the maximum value of the photoelectron peak of Fe (2p) migrated to 711.5 eV. The Fe(III) in solid minerals gradually increased, while Fe(II) gradually decreased and disappeared finally (Fig. 6a–c and Table S2†). The content of the Fe–O increased gradually (Fig. 6d–f and Table S3†). These all indicate that GR_{SO_4} was oxidized, which was caused by electron transfer. The results were consistent with those of XRD, SEM and TEM.

Mechanism and pathway of the reaction

p-CNB, *p*-chlorophenylhydroxylamine and *p*-CAN were detected in this study (Fig. 3 and S1†). Dechlorination did not occur, the nitrogroup was reduced. It is generally thought that the reduction of aromatic nitrogroup to aniline occurs through a series of steps of electron addition and protonation, in which the corresponding aniline is the final product, nitrosobenzene and phenylhydroxylamine are intermediates respectively.[49,50] Therefore, as was shown in Fig. 7, the intermediate products of this experiment should be *p*-nitrosochlorobenzene and *p*-chlorophenylhydroxylamine, and the final product should be *p*-CAN. The stepwise electron addition and protonation happened in this reaction system. In addition to the structural Fe(II) in GR_{SO_4}, dissolved Fe(II) were detected during the reaction (Fig. S3†). The sources of electron donors in the reaction can be divided into the following situations: Fe(II) in the solution, Fe(II) in the structure of GR_{SO_4}. Fe(II) ions with the same concentration of GR_{SO_4} were investigated to reduce *p*-CNB (Fig. S4†). *p*-CNB hardly reacted with Fe(II) alone, the removal efficiencies were less than 4%. Based on the above data, the change of the mineral particles from GR_{SO_4} to goethite and the transformation of Fe(II) to Fe(III) in solid minerals (Fig. 4–6), the electron donor should be structural Fe(II) in GR_{SO_4}, which was consistent with the former study on the reduction of *o*-CNB by GR.[26]

Conclusions

GR_{SO_4} could efficently reduce *p*-CNB. The removal efficiencies and reduction rates of *p*-CNB became higher with the increase of pH value. Ions improved the removals of *p*-CNB. The removal rates of *p*-CNB improved substantially with the presence of CO_3^{2-}. The added NOM could have an adsorption with *p*-CNB. The reduction of *p*-CNB by GR_{SO_4} can only reduce nitro group without dechlorination. The green rust was gradually transformed into goethite. The reduction depended mainly upon the structural Fe(II) in GR_{SO_4}.

Conflicts of interest

There are no conflicts to declare.

Acknowledgements

This research was supported by the National Natural Science Foundation of China (No. 51508510) and Zhejiang Provincial Natural Science Foundation of China (No. LQ15E080009).

References

1 C. R. Jones, Y. Y. Liu, O. Sepai, H. F. Yan and G. Sabbioni, *Environ. Sci. Technol.*, 2006, **40**, 387–394.
2 W. Q. Kong, J. Y. Lin, X. He, Y. Y. Cheng, X. S. Zhang, G. Z. Deng, R. S. Han and C. Wu, *Chemosphere*, 2017, **187**, 62–69.
3 Z. Guo, S. Zheng, Z. Zheng, F. Jiang, W. Hu and L. Ni, *Water Res.*, 2005, **39**, 1174–1182.
4 B. Huang, W. Qian, C. Yu, T. Wang, G. Zeng and C. Lei, *Chem. Eng. J.*, 2016, **306**, 607–618.
5 X. Jiang, J. Shen, Y. Han, S. Lou, W. Han, X. Sun, J. Li, Y. Mu and L. Wang, *Water Res.*, 2016, **88**, 257–265.
6 X. Xu, J. Shao, M. Li, K. Gao, J. Jin and L. Zhu, *Bioresour. Technol.*, 2016, **218**, 1037–1045.
7 D. Colón, E. J. Weber and J. L. Anderson, *Environ. Sci. Technol.*, 2006, **40**, 4976–4982.
8 Z. Guo, J. Liu and F. Liu, *Microporous Mesoporous Mater.*, 2015, **213**, 8–13.
9 L. Zhu, H.-z. Lin, J.-q. Qi, X.-y. Xu and H.-y. Qi, *Water Res.*, 2012, **46**, 6291–6299.
10 J. M. Shen, Z. L. Chen, Z. Z. Xu, X. Y. Li, B. B. Xu and F. Qi, *J. Hazard. Mater.*, 2008, **152**, 1325–1331.
11 M. Ye, Z. Chen, T. Zhang and W. Shao, *Water Sci. Technol.*, 2012, **66**, 479–486.
12 A. H. Pizarro, C. B. Molina, J. A. Casas and J. J. Rodriguez, *Appl. Catal., B*, 2014, **158–159**, 175–181.
13 B. Huang, J. Li, X. Cao, Y. Zhu, W. Chen and C. Lei, *Electrochim. Acta*, 2019, **296**, 980–988.
14 M. Kobayashi, S. Kurosu, R. Yamaguchi and Y. Kawase, *J. Environ. Manage.*, 2017, **200**, 88–96.
15 Y. Zhang, G. B. Douglas, L. Pu, Q. Zhao, Y. Tang, W. Xu, B. Luo, W. Hong, L. Cui and Z. Ye, *Sci. Total Environ.*, 2017, **598**, 1140–1150.
16 M. Elsner, R. P. Schwarzenbach and S. B. Haderlein, *Environ. Sci. Technol.*, 2004, **38**, 799–807.
17 L. Yan and G. W. Bailey, *J. Colloid Interface Sci.*, 2001, **241**, 142–153.
18 J. Cervini-Silva, R. A. Larson, J. Wu and J. W. Stucki, *Environ. Sci. Technol.*, 2001, **35**, 805–809.
19 J. Cervini-Silva, J. Wu, R. A. Larson and J. W. Stucki, *Environ. Sci. Technol.*, 2000, **34**, 915–917.
20 B. C. Christiansen, T. Balic-Zunic, P. O. Petit, C. Frandsen, S. Mørup, H. Geckeis, A. Katerinopoulou and S. L. S. Stipp, *Geochim. Cosmochim. Acta*, 2009, **73**, 3579–3592.
21 M. Mullet, Y. Guillemin and C. Ruby, *J. Solid State Chem.*, 2008, **181**, 81–89.
22 L. Fang, L. Xu, C. Liu, J. Li and L. Z. Huang, *Environ. Int.*, 2019, **129**, 299–307.
23 C. Bhave and S. Shejwalkar, *Int. J. Environ. Sci. Technol.*, 2017, **15**, 1243–1248.
24 M. C. F. Wander, K. M. Rosso and M. A. A. Schoonen, *J. Phys. Chem. C*, 2007, **111**, 11414–11423.
25 W. Yin, J. Ai, L. Z. Huang, D. J. Tobler and H. C. B. Hansen, *Environ. Sci. Technol.*, 2018, **52**, 7876–7883.
26 D. Wu, W. Wang and L. Ma, *J. Tongji Univ. Nat. Sci.*, 2010, **38**, 1473–1477.
27 J. M. R. Génin, A. A. Olowe, P. Refait and L. Simon, *Corros. Sci.*, 1996, **38**, 1751–1762.
28 A. Géhin, C. Ruby, M. Abdelmoula, O. Benali, J. Ghanbaja, P. Refait and J. M. R. Génin, *Solid State Sci.*, 2002, **4**, 61–66.
29 S. Koch and G. Ackermann, *Talanta*, 1992, **39**, 687–691.
30 A. S. Anastácio, B. Harris, H.-I. Yoo, J. D. Fabris and J. W. Stucki, *Geochim. Cosmochim. Acta*, 2008, **72**, 5001–5008.
31 H. Fadrus and J. Maly, *Analyst*, 1975, **100**, 549–554.
32 Y. Liu and J. Wang, *Sci. Total Environ.*, 2019, **671**, 388–403.
33 H. Hayashi, K. Kanie, K. Shinoda, A. Muramatsu, S. Suzuki and H. Sasaki, *Chemosphere*, 2009, **76**, 638–643.
34 C. Ruby, C. Upadhyay, A. Gehin, G. Ona-Nguema and J. M. R. Genin, *Environ. Sci. Technol.*, 2006, **40**, 4696–4702.
35 J. H. Fan, H. W. Wang, D. L. Wu and L. M. Ma, *J. Chem. Technol. Biotechnol.*, 2010, **85**, 1117–1121.
36 P. Larese-Casanova and M. M. Scherer, *Environ. Sci. Technol.*, 2008, **42**, 3975–3981.
37 C. Le, J. H. Wu, S. B. Deng, P. Li, X. D. Wang, N. W. Zhu and P. X. Wu, *Water Sci. Technol.*, 2011, **63**, 1485–1490.
38 C. Ruby, A. Gehin, R. Aissa, J. Ghanbaja, M. Abdelmoula and J. M. R. Génin, *Hyperfine Interact.*, 2006, **167**, 803–807.
39 P. Refait, S. H. Drissi, J. Pytkiewicz and J. M. R. Génin, *Corros. Sci.*, 1997, **39**, 1699–1710.
40 Q. Hao, H. Qiao, C. Zhou, K. Zhang, W. Peng, S. Lu and G. Fu, *Chin. J. Environ. Eng.*, 2016, **10**, 3267–3274.
41 I. D. Kovaios, C. A. Paraskeva and P. G. Koutsoukos, *J. Colloid Interface Sci.*, 2011, **356**, 277–285.
42 Y. Zhang, M. Yin, X. Sun and J. Zhao, *Bioresour. Technol.*, 2020, **307**, 123183.
43 D. Colon, E. J. Weber and J. L. Anderson, *Environ. Sci. Technol.*, 2008, **42**, 6538–6543.
44 J. Klausen, S. P. Troeber, S. B. Haderlein and R. P. Schwarzenbach, *Environ. Sci. Technol.*, 1995, **29**, 2396–2404.
45 P. C. J. Graat, M. A. J. Somers and E. J. Mittemeijer, *Appl. Surf. Sci.*, 1998, **136**, 238–259.
46 A. P. Grosvenor, B. A. Kobe, M. C. Biesinger and N. S. McIntyre, *Surf. Interface Anal.*, 2004, **36**, 1564–1574.
47 R. P. Gupta and S. K. Sen, *Phys. Rev. B: Solid State*, 1975, **12**, 15–19.
48 J. P. H. Perez, H. M. Freeman, J. A. Schuessler and L. G. Benning, *Sci. Total Environ.*, 2019, **648**, 1161–1170.
49 L. Han, L. Yang, H. Wang, X. Hu, Z. Chen and C. Hu, *J. Hazard. Mater.*, 2016, **308**, 208–215.
50 D. Naka, D. Kim and T. J. Strathmann, *Environ. Sci. Technol.*, 2006, **40**, 3006–3012.